



## Implementation of a ray-tracing operator for ground-based GPS Slant Delay observation modeling

Reima Eresmaa,<sup>1</sup> Sean Healy,<sup>2</sup> Heikki Järvinen,<sup>3</sup> and Kirsti Salonen<sup>1</sup>

Received 6 August 2007; revised 22 November 2007; accepted 19 February 2008; published 12 June 2008.

[1] Implementation of an observation-modeling algorithm is necessary in order to make use of Slant Delay (SD) observations, processed from ground-based Global Positioning System (GPS) measurements, in Numerical Weather Prediction (NWP). This article introduces an algorithm for SD observation modeling. The algorithm is an extension of radio-occultation bending-angle observation modeling to ground-based GPS meteorology, and it is based on ray-tracing in a two-dimensional plane. The new algorithm is implemented in the framework of the High Resolution Limited Area Model (HIRLAM) in order to allow comparison with a reference model, that has been published earlier. Only insignificant differences are found between observation minus model background (OmB) statistics of the two implementations. In terms of computational efficiency, the new approach is found to be cheaper to apply in the NWP systems currently in use. However, the computational efficiency of the new implementation is shown to rapidly increase with increasing NWP model resolution.

**Citation:** Eresmaa, R., S. Healy, H. Järvinen, and K. Salonen (2008), Implementation of a ray-tracing operator for ground-based GPS Slant Delay observation modeling, *J. Geophys. Res.*, 113, D11114, doi:10.1029/2007JD009256.

### 1. Introduction

[2] Atmospheric refractivity decreases microwave propagation speed and causes tropospheric delay, which influences applications of the Global Navigation Satellite System (GNSS) [e.g., *Bevis et al.*, 1992; *Elgered et al.*, 2005]. Geodetic processing of ground-based measurements from a continuously operating Global Positioning System (GPS) receiver network allows one to estimate tropospheric delays on slanted signal paths through the atmosphere. These estimates are referred to as Slant Delay (SD) observations and they are considered as a potential observation type for operational Numerical Weather Prediction (NWP) systems in future [*de Haan et al.*, 2002; *Ha et al.*, 2003; *Liu and Xue*, 2006; *Järvinen et al.*, 2007].

[3] Development of limited area NWP systems currently aims at modeling of mesoscale phenomena with life-times of a few hours and horizontal scales of some tens of kilometers. The observing systems used in the present operational NWP systems are not believed to be sufficient in order to provide information in these scales. Therefore increased spatial and temporal resolution is required from the future observing networks. Various methods based on remote sensing technology are recognized to carry potential

to fulfill such requirements [e.g., *Schmetz et al.*, 2002; *Le Marshall et al.*, 2002; *Feltz et al.*, 2003].

[4] Remote sensing measurements are typically indirect observations of the NWP model variables. Observation modeling provides a tool for data assimilation of such observations [*Andersson et al.*, 1994; *Derber and Wu*, 1998; *Chevallier et al.*, 2004]. In data assimilation framework, the algorithm performing observation modeling is called an observation operator. Modeling of SD observations consists of numerical integration of atmospheric refractivity along the signal path [*Eresmaa and Järvinen*, 2006]. However, since the signal path depends on the three-dimensional refractivity distribution, the observation modeling is more complicated than a mere numerical integration. Determination of the signal path needs to be performed as part of the observation modeling.

[5] Methodological development is taking place on data assimilation of bending-angle observations processed from GPS radio occultation (RO) measurements [*Poli and Joiner*, 2004; *Healy et al.*, 2007]. These observations have been shown to have a positive impact on global NWP forecasts [*Healy and Thépaut*, 2006]. The impact is particularly pronounced in analysis of stratospheric and upper tropospheric temperature. Observation modeling of the GPS RO observations involves determination of the GPS signal path in a two-dimensional plane as a solution to a set of partial differential equations.

[6] In this article, the approach used for GPS RO observation modeling is extended to modeling of ground-based GPS slant delay observations. Instead of a satellite-to-satellite signal path, a satellite-to-ground-based receiver signal path is considered with essentially the same algorithm as is used for GPS RO observation modeling. The

<sup>1</sup>Research and Development, Meteorology, Finnish Meteorological Institute, Helsinki, Finland.

<sup>2</sup>European Centre for Medium-ranged Weather Forecasts, Research Department, Data Division, Reading, UK.

<sup>3</sup>Research and Development, Climate Change, Finnish Meteorological Institute, Helsinki, Finland.

new SD observation modeling algorithm is implemented in the framework the High Resolution Limited Area Model (HIRLAM; *Undén et al.* [2002]), and it is compared with a reference model that has been published earlier [*Eresmaa and Järvinen*, 2006]. The new algorithm is described and the reference model is outlined in section 2. Later sections focus on validating the new implementation by means of observation minus model background (OmB) statistics (section 3), behavior of modeled SD at very large satellite zenith angles (section 4), and computational efficiency (section 5). The implications of the results in variational data assimilation in general and in weather radar observation modeling are discussed in section 6, followed by conclusions drawn in section 7.

## 2. SD Observation Modeling

[7] This section describes the modeling of SD in the framework of the HIRLAM NWP system. The analysis system of HIRLAM is based on variational data assimilation (HIRLAM 3/4D-Var [*Gustafsson et al.*, 2001; *Lindskog et al.*, 2001]). The variational data assimilation algorithms use iterative methods to find the NWP model state  $\mathbf{x}$  which minimizes the cost function

$$J(\mathbf{x}) = \frac{1}{2}(\mathbf{x} - \mathbf{x}_b)^T \mathbf{B}^{-1}(\mathbf{x} - \mathbf{x}_b) + \frac{1}{2}(\mathbf{y} - H\mathbf{x})^T \mathbf{R}^{-1}(\mathbf{y} - H\mathbf{x}), \quad (1)$$

where  $\mathbf{x}_b$  is the background field,  $\mathbf{y}$  is the vector consisting of observations,  $H$  is the observation operator, and  $\mathbf{B}$  and  $\mathbf{R}$  are the background and observation error covariance matrices, respectively. The background field  $\mathbf{x}_b$  is a short-term forecast from the previous analysis cycle. In addition to the nonlinear observation operator  $H$ , the iterative minimization of the cost function (1) makes use of the tangent linear and adjoint versions of the observation operator.

[8] The NWP model state vector  $\mathbf{x}$  of the HIRLAM 3D-Var consists of the grid point values of temperature ( $T$ ), specific humidity ( $q$ ), horizontal wind components ( $u$ ,  $v$ ) and logarithm of surface pressure ( $\ln p_s$ ). Pressure  $p$  at the NWP model levels follows uniquely from the NWP model variables under the hydrostatic assumption.

### 2.1. Tropospheric Refraction

[9] The effect of the neutral atmosphere on GPS signal propagation is referred to as tropospheric refraction [e.g., *Hofmann-Wellenhof et al.*, 2001]. The SD observation operators are built upon the definition of the excess path length due to tropospheric refraction,

$$SD = \int_s n ds - \int_g dg = \int_s (n - 1) ds + \left( \int_s ds - \int_g dg \right), \quad (2)$$

where  $s$  is the signal path through the atmosphere,  $n$  is the real part of the atmospheric refractive index, and  $g$  is the

geometrical signal path that would occur in the hypothetical case of no atmosphere affecting the signal propagation. Definition (2) shows that SD arises from deviations of  $n$  from unity along  $s$  (the first term on the right-hand-side) on the one hand, and from the increase of the signal path length due to tropospheric refraction (the remaining terms) on the other. The latter effect is sometimes called geometric delay [*Elgered et al.*, 2005]. As this phenomenon is of importance only at large zenith angles, the definition (2) is often approximated as

$$SD \approx \int_s (n - 1) ds = 10^{-6} \int_s N ds, \quad (3)$$

where  $N = 10^6(n - 1)$  is called refractivity.

[10] Making use of the ideal gas assumption allows one to derive a relationship

$$N = k_1 \frac{p_d}{T} + k_2 \frac{e}{T} + k_3 \frac{e}{T^2} \quad (4)$$

for  $N$  at microwave frequencies [*Bevis et al.*, 1992]. Refractivity is thus a function of dry air and water vapor pressures ( $p_d$  and  $e$ ) and temperature ( $T$ ). As shown by *Eresmaa and Järvinen* [2006], (4) can be further modified to

$$N = \frac{k_1 p}{T} + \frac{(k_2 - k_1) q p}{(0.622 + 0.378 q) T} + \frac{k_3 q p}{(0.622 + 0.378 q) T^2}. \quad (5)$$

This study applies values suggested by *Bevis et al.* [1994] for the refractivity coefficients. These are  $k_1 = 77.60 \text{ K hPa}^{-1}$ ,  $k_2 = 70.4 \text{ K hPa}^{-1}$  and  $k_3 = 3.739 \times 10^{-5} \text{ K}^2 \text{ hPa}^{-1}$ .

### 2.2. New Algorithm

[11] The new approach for the SD observation modeling is based on a two-dimensional ray-tracing code that is originally developed for data assimilation of GPS RO bending angle measurements [*Healy et al.*, 2007], following *Rodgers* [2000]. This approach is hereafter referred to as the Least Traveltime (LTT) algorithm. Motivation for this convention follows from the fact that the ray-tracing method searches for the signal path that provides the shortest possible traveling time from the transmitter to the receiver.

[12] The LTT algorithm operates on a two-dimensional plane that is defined by the center of the Earth, the ground-based receiver and the GPS satellite. Each signal path element lies on this plane, at a radius  $r$  from the center of the Earth and at an angular separation  $\psi$  to an arbitrary reference direction. The coordinates of the receiver and the satellite are denoted by  $(r_{rec}, \psi_{rec})$  and  $(r_{sat}, \psi_{sat})$ , respectively. The reference direction is chosen such that  $\psi_{rec} = 0$ .

[13] The input to the LTT algorithm consists of a two-dimensional array of refractivity as a function of radius  $r$  and angular separation  $\psi$ , as interpolated to the two-dimensional plane from the three-dimensional NWP model state. The signal path is obtained as a set of path elements  $(r, \psi)$ , which satisfy the differential equations

$$\frac{dr}{ds} = \cos \theta, \quad (6)$$

$$\frac{d\psi}{ds} = \frac{\sin\theta}{r}, \text{ and} \quad (7)$$

$$\frac{d\theta}{ds} \simeq -\sin\theta \left[ \frac{1}{r} + \left( \frac{\partial n}{\partial r} \right)_{\psi} \right]. \quad (8)$$

where  $s$  is the distance along the signal path, and  $\theta$  is the angle between the local radius vector and the tangent to the signal path (local zenith angle), see Figure 9.2 by *Rodgers* [2000]. The equations are solved here with a fourth-order Runge-Kutta method. It is assumed that the refractivity decays exponentially with increasing height between two adjacent NWP model levels.

[14] The signal path calculation is started at  $(r_{rec}, \psi_{rec})$  and it is continued until  $r_{sat}$  is reached. Since the atmospheric effect to signal propagation varies from time to time, the zenith angle  $\theta_{rec}$  at  $(r_{rec}, \psi_{rec})$  is not known prior to SD modeling and signal path determination. Therefore  $\theta_{rec}$  is first set equal to the geometrical zenith angle  $\theta_g$  of the satellite, i.e., the zenith angle at which the satellite would be seen in the hypothetical case of no atmosphere affecting the signal propagation. As the signal path calculation proceeds toward higher altitudes, the modeled SD is aggregated by integrating the refractivity along the signal path by the Runge-Kutta solver. Contribution of SD from above the NWP model top is modeled with the Saastamoinen formula [Saastamoinen, 1972].

[15] As  $\theta_{rec}$  is initially set equal to the geometrical zenith angle of the satellite, the resulting signal path will generally not meet the satellite. In other words, the angular separation  $\psi$  of a signal path element at  $r_{sat}$  will be different from  $\psi_{sat}$ . Therefore the calculation of the signal path and SD is repeated by using an updated  $\theta_{rec}$ . The update reduces  $\theta_{rec}$  to account for the signal path bending. The final SD is approximated as a linear combination of the two estimates through

$$SD = wSD_1 + (1 - w)SD_2 \quad (9)$$

where  $SD_1$  and  $SD_2$  are the slant delays calculated for the first and the second signal path, respectively. The weighting  $w$  is given by

$$w = \frac{\psi_2 - \psi_{sat}}{\psi_2 - \psi_1} \quad (10)$$

where  $\psi_1$  and  $\psi_2$  are the angular separations of the endpoints of the two signal paths, respectively. In principle, the accuracy of the LTT algorithm could be further increased by searching the optimal  $\theta_{rec}$  iteratively on the cost of increased computing time.

### 2.3. Reference Model

[16] The Geometrical Path Corrected (GPC) model [Eresmaa and Järvinen, 2006] provides a reference for validation of the new implementation in this article. In the GPC model, the geometrical signal path  $g$ , that appears in equation (2), is used as a starting point for the signal path determination. The main assumption of the GPC model is that a sufficient accuracy for the signal path determination

can be achieved by applying an explicit refractivity-dependent correction to the geometrical zenith angle. The signal path  $s$  is defined as a set of coordinates of the intersections of  $s$  with each of the NWP model levels.

[17] The explicit correction for the refractive bending is based on the Snell's law of wave propagation. It is assumed that the apparent zenith angle  $\theta_a$  is only a function of the geometrical zenith angle  $\theta_g$  and the refractivity  $N$  through

$$\sin\theta_a = \frac{\sin\theta_g}{n} = \frac{\sin\theta_g}{10^{-6}N + 1}. \quad (11)$$

The apparent zenith angle is calculated separately at each NWP model level – signal path intersection.

[18] Note that the explicit correction makes the process of signal path determination iterative. This follows from the fact that the intersection coordinates depend on refractivities at the intersections and vice versa. In practice, it is found sufficient to carry out the intersection determination twice. Equation (11) is then applied only during the second iteration step, after determining the approximate  $N$  during the first iteration step. The iteration decreases the computational efficiency of the GPC model.

[19] Once the signal path intersections are determined, the NWP model variables are interpolated to the intersections using bilinear interpolation method, and the refractivity at the intersections is determined by applying equation (5). SD is obtained as a numerical integral of equation (3) through the following procedure.

[20] (1) For each layer  $i$  between two adjacent NWP model levels, the parameters  $a_i$  and  $b_i$  of

$$N = \exp(a_i + b_i z), \quad (12)$$

are solved separately. In equation (12),  $z$  is the intersection height. As both  $N$  and  $z$  at the top and at the bottom of each layer are known, this parameter determination is unique.

[21] (2) Equation (12) is substituted in equation (3) and integrated analytically (with respect to  $z$ ) in each layer. This results in

$$10^{-6} \int_{z_{i+1}}^{z_i} N dz = \frac{\exp(a_i + b_i z_i) - \exp(a_i + b_i z_{i+1})}{10^6 b_i}, \quad (13)$$

where  $z_{i+1}$  and  $z_i$  are the heights of the intersections  $i+1$  and  $i$ , respectively. These determine the lower and the upper boundaries of the layer  $i$ .

[22] (3) In each layer  $i$ , the integral (13) is scaled by the cosine of the apparent zenith angle  $\theta_{a,i}$  in order to account for the slanted signal path. This scaling provides the contribution  $SD_i$  originating from the layer  $i$ :

$$SD_i = \frac{\exp(a_i + b_i z_i) - \exp(a_i + b_i z_{i+1})}{10^6 b_i \cos\theta_{a,i}}. \quad (14)$$

[23] (4) Contributions from all layers in vertical are summed up to obtain the total NWP model resolved SD.

[24] (5) The contribution from above the NWP model top as determined by the Saastamoinen formula [Saastamoinen, 1972] is added to complete the SD determination.

**Table 1.** Summary of the Assumptions Made in the Two Modeling Algorithms

---

<i>Assumptions that are common to the two algorithms</i>
SD is only a function of pressure, temperature and specific humidity along the signal path, i.e., contributions of e.g., aerosols and liquid water are negligible. Geometric delay is considered negligible, i.e., $(\int_s ds - \int_g dg) = 0$ .
Air is approximated as an ideal gas.
Values suggested by <i>Bevis et al.</i> [1994] are used for $k_1$ , $k_2$ and $k_3$ .
Refractivity decays exponentially between two adjacent NWP model levels.
The formula of <i>Saastamoinen</i> [1972] is used for SD contribution from above the NWP model top.
<i>Assumptions that are specific to the LTT algorithm</i>
The signal path is restricted to the two-dimensional plane determined by the satellite, the receiver and the center of the Earth.
SD is a linear combination of two preliminary estimates that differ in terms of the zenith angle at the receiver.
The signal path and SD are computed simultaneously.
<i>Assumptions that are specific to the GPC algorithm</i>
The apparent zenith angle follows from the geometrical zenith angle and refractivity at a single point.
The signal path between two adjacent NWP model levels is a straight geometric line.
The signal path does not face essential modifications during the minimization of the 3D- or 4D-Var cost function (the signal path and SD are computed separately).

---

## 2.4. Summary of the Differences Between the Algorithms

[25] Table 1 summarizes the assumptions and approximations that are made in the GPC and LTT algorithms. There are three fundamental differences that can be pointed out between the two SD modeling algorithms. The differences relate to the task of signal path determination; integration of the refractivity to yield the modeled SD is performed essentially in a similar manner by the two algorithms. The differences in the signal path determination are discussed next.

[26] The first difference is that while the LTT algorithm operates on NWP model refractivity as interpolated in a two-dimensional array, the GPC model operates on the full three-dimensional NWP model grid of pressure, temperature and specific humidity. The input to the LTT algorithm is thus substantially reduced as compared with the input to the GPC model.

[27] Second, the GPC model provides an explicit signal path, i.e., a set of three-dimensional coordinates that define the signal path. Once the signal path is determined (after the second iteration as discussed in section 2.3), it is kept fixed until the end of the data assimilation. Even though the minimization of the cost function modifies the NWP model state, the signal path is not modified. The treatment of the signal path in the LTT algorithm is rather different. In the LTT algorithm, the signal path is fully governed by the differential equations (6)–(8), and the path is therefore modified also during the minimization of the 3D- or 4D-Var cost function.

[28] Third, the GPC model applies the Snell's law of wave propagation in order to provide an explicit correction to the geometrical satellite zenith angle. The LTT algorithm, in contrast, determines SD as a linear combination of two preliminary estimates. It is assumed that the weighting, that is based on the angular separations of the two signal paths at  $r_{sat}$ , correctly accounts for the effect of refractive bending.

## 3. Accuracy of SD Modeling

[29] This section provides an analysis of modeling accuracy of the LTT model as compared with that of the

referencing GPC model. The two implementations are applied to HIRLAM NWP model output.

### 3.1. HIRLAM NWP Model Output

[30] Three hour numerical forecasts of  $\ln p_s$ ,  $T$  and  $q$  are retrieved from the output of the HIRLAM NWP model on 40 levels in vertical. Two horizontal resolutions, corresponding to grid spacings of 11 and 5.6 km, respectively, are used. This extends the assessment to the impact of changing the horizontal resolution of the NWP model. The modeling domains are shown in Figure 1. The boundary conditions for the limited area NWP model are retrieved from HIRLAM analyses of a coarser resolution (grid spacing 22 km) run. The analysis cycling is 3 h. Only conventional observation types including TEMP, PILOT, SYNOP, SHIP, AIREP and DRIBU observations are used in data assimilation.

### 3.2. SD Observation Data Set

[31] The SD observations for the validation are preprocessed at the Technical University of Delft, Netherlands [*de Haan et al.*, 2002]. The data set spans over time period of 1–24 May 2003. This study utilizes data from 15 GPS receiver stations located at a sufficiently large distance from the lateral boundary of the inner NWP model domain, such that all signal paths are entirely within the NWP model lateral boundaries. The receiver station locations are shown in Figure 1. The temporally thinned data set gathers observations at 10 minute time interval. Intermediate data is not used. With this experiment setup, a subset of 280 149 SD observations enters the validation.

[32] The preprocessing of SD observations makes use of two fundamental assumptions. First, the fitting residuals of the geodetic network solution are interpreted as the azimuthally asymmetric contribution of SD. Second, it is assumed that the effect of signal multipath propagation can be accurately modeled by so-called multipath maps, which are constructed by averaging the fitting residuals over a time period of several days. The multipath maps are generated separately for each receiver station and they represent the multipath effect at different azimuth and zenith angles. Under these assumptions the preprocessing of SD observations is started by collecting raw GPS pseudorange

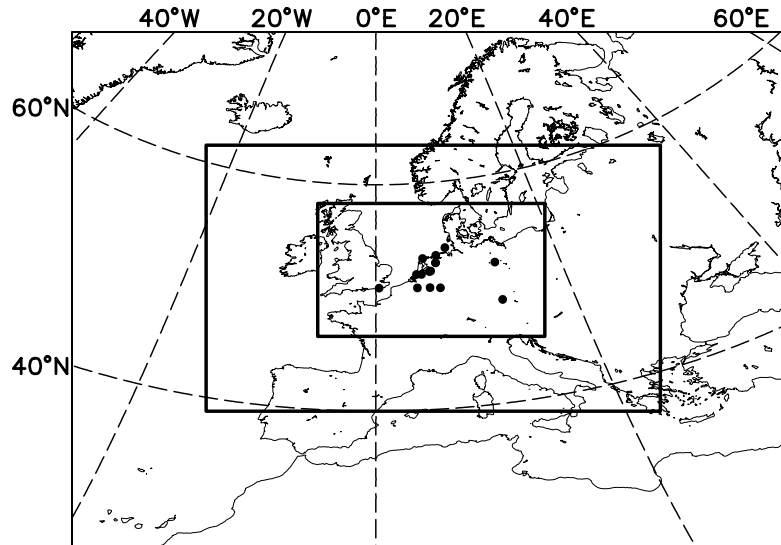


**Figure 1.** HIRLAM domains used in the NWP model runs with 11 km (outer rectangle) and 5.6 km (inner rectangle) grid spacings. The dots indicate the locations of the ground-based GPS receiver stations used in this study.

measurements over a time interval of 20 min. The raw measurements are processed by the Bernese GPS processing software [Hugentobler *et al.*, 2001] in order to obtain the hydrostatic and wet zenith delay contributions at each receiver station. Together with the Niell [1996] hydrostatic and wet mapping function values corresponding to a given satellite zenith angle, the zenith delays determine the symmetric component of SD. Preprocessed SD is then obtained as a linear combination

$$SD = m_h ZHD + m_w ZWD + \delta_r^s - M(\alpha, \theta), \quad (15)$$

where  $m_h$  and  $m_w$  are the hydrostatic and wet mapping functions, ZHD and ZWD are the zenith hydrostatic and wet delays determined within the preprocessing,  $\delta_r^s$  is the fitting residual of the pseudorange measurement between the satellite  $s$  and the receiver  $r$ , and  $M(\alpha, \theta)$  is the multipath modeled as a function of azimuth  $\alpha$  and zenith angles  $\theta$ .

### 3.3. OmB Statistics

[33] Observation minus background (OmB) departure is a composite of observation, modeling and background errors. A statistical analysis of OmB provides information on the statistical properties of these error contributions. In this section, the OmB statistics of the LTT model are compared with those of the GPC model. Since the same observations and background fields are applied to both implementations, all differences that are revealed are concluded to be due to different errors in observation modeling. OmB mean and standard deviations are calculated over the whole subset of SD observations. Statistics of individual receiver stations are not studied.

[34] Figure 2 shows these statistics, corresponding to the HIRLAM run at 5.6 km grid spacing, as a function of satellite zenith angle. The mean OmB increases uniformly with increasing zenith angle and reaches the thresholds of 2, 3, and 4 cm at zenith angles 55°, 67°, and 73°, respectively. The curves of the two observation operators are practically

identical at zenith angles smaller than 75°. As the zenith angle is increased beyond 75°, the LTT model (solid line) appears to be slightly closer to the observations than the GPC model (dashed line).

[35] Figure 2 shows also the standard deviation of OmB for the LTT model (dash-dotted line). The standard deviation of OmB for the GPC model is practically identical and is not shown. The similarity of the standard deviations suggests that random modeling errors of the LTT model are identical to those of the GPC model in statistical sense. For most satellite zenith angles, the OmB standard deviation is larger than the OmB mean. Moreover, the OmB standard deviation increases uniformly with increasing zenith angle and reaches the level of 7–8 cm at the largest zenith angles. The OmB mean is relatively close to the OmB standard deviation, which means that there are significantly more positive than negative OmB values. In fact, the proportion

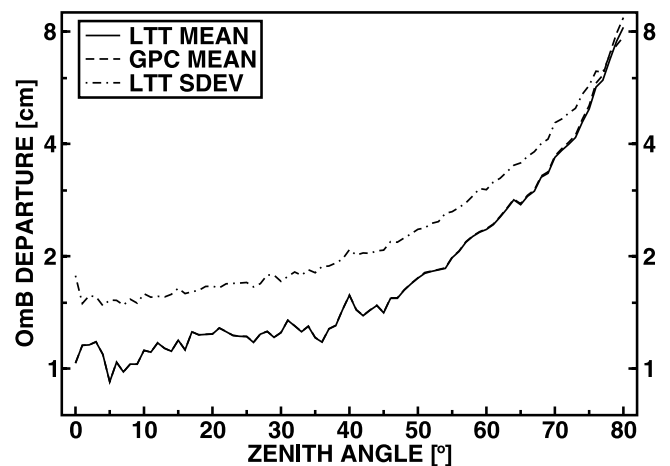


**Figure 2.** Mean OmB for LTT (solid line), mean OmB for GPC (dashed line) and standard deviation of OmB for LTT (dash-dotted line) as a function of satellite zenith angle.

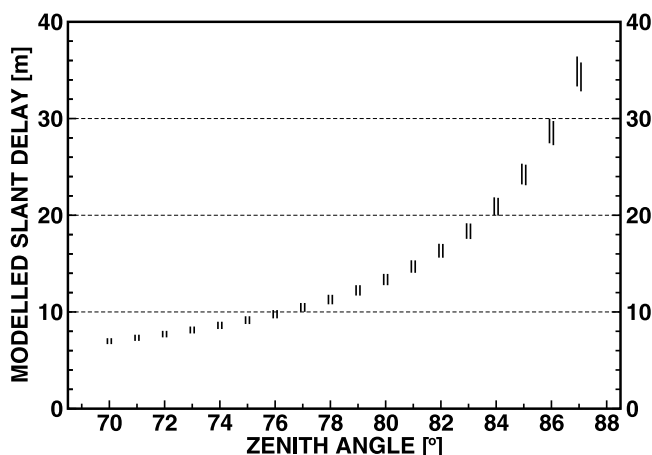


**Figure 3.** Range of SD at different satellite zenith angles as modeled by using LTT (left bars) and GPC (right bars) models.

of the positive OmB values turns out to be more than 80%. As the data assimilation algorithms usually assume unbiased observations and background field, the proportion of positive OmB values should in the optimal case be about 50%. Therefore a development and implementation of a bias correction scheme is considered necessary prior to extensive SD data assimilation experiments, unless significant breakthroughs are achieved in the forward modeling and/or preprocessing of SD observations.

[36] The mean and standard deviation of OmB are studied also corresponding to the NWP model run at 11 km grid spacing (not shown). Again, the statistics of the LTT model are practically the same as those of the GPC model. However, the decrease in the horizontal resolution results in a few millimeters increase in both the mean and the standard deviation of OmB, in particular at relatively large satellite zenith angles. This is considered reasonable as decreasing horizontal resolution implies, on the one hand, less accurate NWP model physiography, and, on the other hand, a larger contribution of subgrid-scale atmospheric circulations that are too small to be represented by the NWP model grid.

#### 4. Behavior of Modeled SD at Large Satellite Zenith Angles

[37] The preprocessing of the SD observations has been performed applying a satellite zenith angle cutoff of  $80^\circ$ . The tuning of the cutoff angle is a trade-off between increase of asymmetry of the SD observations with increasing zenith angle [Eresmaa et al., 2007] and the increasing measurement noise combined with the disturbing effect of multipath propagation at very large zenith angles. The data set allows no comparison with observations at zenith angles larger than the cutoff angle. Since the mean OmB curves of Figure 2 suggest existence of a systematic difference between SD modeled by either the LTT or the GPC implementation at large satellite zenith angles, the LTT model is next compared with the GPC model in terms of behavior of modeled SD as zenith angle is increased beyond  $80^\circ$ . The adopted procedure is as follows.

[38] Twenty four 3-h HIRLAM forecasts at 5.6 km horizontal grid spacing are used. Each forecast is valid at 15 UTC during 1–24 May 2003. Using forecast experiment spanning over a time period of several weeks is believed to improve the representativeness of the results, as various synoptic situations are covered. The hypothetical observing network consists of 10 GPS receiver stations, which are located near the center of the NWP model domain. Each station is assumed to observe 18 satellites at zenith angles  $70^\circ, 71^\circ, 72^\circ, \dots, 87^\circ$  at the azimuth angle of  $0^\circ$  (north). NWP model counterparts are calculated for the hypothetical observations by the two implementations. Finally, the NWP model counterparts are intercompared at each zenith angle.

[39] Figure 3 shows the range of the NWP model counterparts at each satellite zenith angle. There are 240 observations at each zenith angle. No detectable differences between the two implementations can be seen at zenith angles smaller than  $80^\circ$ . Increasingly large differences can, however, be pointed out as soon as the zenith angle exceeds  $81^\circ$ – $82^\circ$ . At the largest zenith angles, the LTT model (left bars at each zenith angle bin) provides systematically larger values for SD than does the GPC model (right bars). A more quantitative intercomparison (not shown) reveals that the mean difference (LTT-GPC) is 0.5 cm at  $80^\circ$ , 9.6 cm at  $85^\circ$  and 55.8 cm at  $87^\circ$ .

[40] As the main difference between the two implementations is in the signal path determination and since the LTT model is considered more sophisticated in this sense, it is believed that the systematic difference between the modeled SD results from inaccuracy of the referencing GPC model. The interpretation is that the explicit correction applied by the referencing GPC model overestimates the effect of refractive bending. This leads to too small values of apparent zenith angle at signal path intersections, and moreover to too small SD contributions for each layer between two adjacent NWP model levels. As a result, a too small value is obtained for SD.

#### 5. Computational Efficiency

[41] From the operational NWP point of view, it is essential that the numerical analysis and forecast output can be generated within a time frame of only a few hours after the nominal analysis time. As there might be several thousands of SD observations to be assimilated into a single analysis in future, it is important that the observation operator is computationally efficient. The performances of the LTT and the GPC implementations are next assessed in terms of computational efficiency, i.e., the mean computing time of a NWP model counterpart. The mean computing time is calculated in a Linux PC environment using the following experiment design.

[42] A series of computer runs are performed in order to study the dependence of the computing time on the horizontal grid resolution of the NWP model on the one hand and the satellite zenith angle on the other. Each run determines mean computing time at a given implementation (LTT or GPC), at a given grid resolution (11, 5.6 or 2.8 km grid spacing) and at a given satellite zenith angle ( $10^\circ, 20^\circ, 30^\circ, 40^\circ, 50^\circ, 55^\circ, 60^\circ, 65^\circ, 70^\circ, 75^\circ, 80^\circ$ , or  $85^\circ$ ). In this experiment, SD observing network is assumed to consist of 10 GPS receiver stations located near the center of the NWP

**Table 2.** Mean Computing Time in Milliseconds of a Single SD Model Counterpart at Different Satellite Zenith Angles With NWP Grid Spacings of 11, 5.6 and 2.8 km<sup>a</sup>

Zenith Angle	11 km		5.6 km		2.8 km	
	LTT	GPC	LTT	GPC	LTT	GPC
10°	1.31	2.01	1.31	2.02	1.35	2.03
20°	1.27	2.02	1.39	2.03	1.43	2.06
30°	1.31	2.02	1.39	2.03	1.50	2.07
40°	1.35	2.10	1.42	2.13	1.65	2.11
50°	1.45	2.14	1.58	2.07	1.89	2.14
55°	1.45	2.03	1.74	2.09	<b>2.02</b>	<b>2.22</b>
60°	1.49	2.03	1.72	2.10	2.23	2.20
65°	1.56	2.04	1.79	2.19	2.42	2.23
70°	1.62	2.05	<b>1.94</b>	<b>2.12</b>	2.69	2.22
75°	1.72	2.06	2.18	2.15	3.19	2.35
80°	<b>1.99</b>	<b>2.07</b>	2.73	2.19	4.33	2.34
85°	2.74	2.10	4.34	2.28	7.44	2.46

<sup>a</sup>Records for the largest zenith angle at which the LTT model performs faster are typed in bold face.

model domain, and each receiver station is assumed to provide one SD observation at each satellite zenith angle. Since the computer is simultaneously running several background processes that are not controlled by the experiment, the computing time of a single NWP model counterpart is, to some extent, subject to random fluctuations. Therefore the computation of each NWP model counterpart is repeated 1000 times, and only the mean computing times are taken under consideration.

[43] The mean computing times, in milliseconds, at different grid resolutions and satellite zenith angles are given in Table 2. For both the LTT and the GPC models, the mean computing time increases with increasing zenith angle. In the case of the LTT model, the increase becomes steeper toward the largest zenith angles. The increase of computing time is much more uniform in the case of the referencing GPC model.

[44] The mean computing time increases also with decreasing grid spacing. Again, the increase is steeper for the LTT than for the GPC model. At relatively small zenith angles, the LTT model is more efficient than the GPC model. The largest zenith angle at which this is true are highlighted in Table 2 for each grid spacing. At a grid spacing of 11 km, the LTT model is practically always faster than the GPC model. As grid spacing is reduced to 2.8 km, the LTT model loses this advantage for the satellite zenith angles larger than 55°.

[45] Real GPS satellite constellations are irregular and vary in time, and the satellites are unevenly distributed at different zenith angles. Usually, there are relatively more satellites visible at large zenith angles. The computational efficiencies are therefore next investigated in real observation geometries appearing at the permanent GPS receiver station of Metsähovi, Finland (60.22°N, 24.40°E) every tenth minute during 16–18 September 2005. Applying satellite zenith angle cutoffs of 75°, 80° and 85°, the number of signal paths to be modeled is 3229, 3860 and 4425, respectively. Time spent by each implementation for modeling the SD observations at each grid resolution is estimated using Table 2. For intermediate zenith angles, computing times are obtained by using linear interpolation from the two closest zenith angles appearing in Table 2.

[46] Ratio of the time spent by the LTT model for SD modeling divided by the time spent by the GPC model is given in Table 3 for different zenith angle cutoffs and grid resolutions. As the satellite zenith angle cutoff is increased, the ratio increases. This means that the LTT model loses its efficiency with respect to the GPC model. The LTT model performs faster at all satellite zenith angle cutoffs at grid resolutions of 11 and 5.6 km. At 2.8 km grid resolution, the GPC model is faster if satellite zenith angle cutoff is at least 80°. Since the potential of SD observations lies mostly in kilometer-scale NWP [Eresmaa *et al.*, 2007], it is concluded that the two implementations are essentially equally efficient for forward modeling of SD observations.

[47] The dependence of the computing time of the LTT model to satellite zenith angle and grid spacing results from the varying dimension of the two-dimensional refractivity field, which is given as an input to the ray-tracing algorithm. The time taken by the ray tracing itself is probably independent of zenith angle and grid spacing. In contrast, the time taken by generating the input and passing it to the algorithm depends on dimension of the field. The larger the zenith angle and the denser the NWP model grid, the more vertical refractivity profiles are needed for ray tracing, the larger is the dimension of the input field, and the more time is spent in this step. The GPC model does not show this kind of dependence, because it operates on the full three-dimensional NWP model fields.

## 6. Discussion

[48] The validation results presented in this article focus on the nonlinear versions of the LTT and GPC models. In variational data assimilation, the minimization of the 3D- or 4D-Var cost function additionally makes use of the tangent-linear and adjoint versions of the observation operators. Since the treatment of the signal path in the LTT model is fundamentally different from that in the GPC model, it is likely that the conclusions on the computational efficiencies of the tangent-linear and adjoint operators would be quite different from those of the nonlinear operator. In the case of the GPC model, the time spent by the observation modeling is dominated by the time spent by the signal path determination. However, this task is not repeated by the tangent-linear or adjoint operators. Therefore the tangent-linear and adjoint operators spend only a small fraction of the time spent by the nonlinear operator. In the case of the LTT model, in contrast, the tangent-linear and the adjoint operators perform exactly the same tasks as the nonlinear operator. As there can be up to one hundred evaluations of the cost function and its gradient, and all of these evaluations involve performing the tangent-linear and adjoint operators, the time taken by the data assimilation of

**Table 3.** Ratio of the Time Spent by the LTT Model Divided by the Time Spent by the GPC Model for SD Modeling in Real Observation Geometry at Different Satellite Zenith Angle Cutoffs and NWP Grid Spacings

Zenith Angle Cutoff	11 km	5.6 km	2.8 km
75°	0.711	0.790	0.956
80°	0.742	0.848	1.070
85°	0.793	0.946	1.259

SD observations using the LTT model is likely to be multifold compared to that taken by the GPC model.

[49] Considering the computing times, one should bear in mind that the total computing time spent by the data assimilation is multifold compared to the computing time spent by the SD observation modeling alone. At the moment, the analysis step of a typical HIRLAM experiment with a realistic NWP model configuration spends approximately 15 min of CPU time on a parallelized super computer. Given that the mean computing time of an SD model counterpart is roughly 2 ms, modeling of, for example, 5000 SD observations takes about 10 s of CPU time. This is only slightly more than one percent of the total CPU time spent by the data assimilation.

[50] The signal path determination algorithms designed for SD observations have potential applications also outside the GPS meteorology. For instance, observation modeling for weather radar data can benefit of the path determination algorithm. In the ICAO standard atmosphere conditions the weather radar microwave pulse propagates according to the  $4r/3$ -law, where  $r$  is the Earth's radius [Doviak and Zrnić, 1993]. In varying atmospheric refraction conditions the weather radar microwave pulse propagation deviates from the standard solution. Weather radar observation modeling can thus be improved using integrated refraction of the NWP model state. The GPC algorithm is considered better suited than the LTT algorithm for this application, because only the antenna elevation angle but not the exact altitude of the return scattering received by the radar is known. A common microwave pulse path determination core routine could be applied by both SD and weather radar data (e.g., Doppler radar radial winds and reflectivities).

## 7. Conclusions

[51] This study introduces a new approach for slant delay (SD) observation modeling. This approach, referred to as least traveltime (LTT) algorithm, is an extension of the algorithms applied earlier to bending-angle observations processed from GPS radio occultation (RO) measurements. The LTT algorithm is implemented in the framework of the High Resolution Limited Area Model (HIRLAM) and validated against the reference model (Geometrical Path Corrected, GPC) in terms of observation minus background (OmB) statistics, behavior of modeled SD at large satellite zenith angles, and computational efficiency. The conclusions from the validation are as follows.

[52] (1) The modeling accuracy of the LTT implementation is practically identical to that of the GPC model. A hardly noticeable improvement can be pointed out in the mean OmB (bias) at satellite zenith angles larger than  $75^\circ$ . The OmB standard deviations of the two implementations are similar.

[53] (2) As satellite zenith angle increases beyond  $80^\circ$ , the difference between the SD's modeled by the two implementations starts to increase rapidly and reaches 10 cm at the zenith angle of  $85^\circ$  and 50 cm at the zenith angle of  $87^\circ$ . The interpretation of this is that the LTT model is more accurate in accounting for refractive bending.

[54] (3) In the case of nonlinear observation modeling, the computing times corresponding to the two observation operators are roughly the same. At relatively low satellite

zenith angles and with a relatively coarse NWP model grid, the new LTT model performs faster. However, the increase of computing time with increasing zenith angle and grid resolution is considerably steeper for the LTT model than for the referencing GPC model.

[55] It is summarized that the new LTT approach for SD observation modeling is computationally feasible and provides a similar or even better modeling accuracy than the reference GPC model. The LTT model is expected to perform better in particular in those cases, where SD observations from satellite zenith angles larger than  $80^\circ$  are available. However, this can only be achieved with the cost of increased computing time. Moreover, the computing time of the LTT model is further increased if the NWP model grid spacing is reduced. As a recent study reported by Eresmaa *et al.* [2007] suggests that benefiting of SD observations in NWP requires such a high horizontal resolution, the feasibility of the referencing GPC model is concluded to be maintained.

[56] **Acknowledgments.** The funding from the EU FP5 project "Targeting Optimal Use of GPS Humidity Measurements in Meteorology" (TOUGH) in 2003–2006 and from the TEKES project "Geophysically Assisted Satellite Positioning" in 2004–2006 is thankfully acknowledged. TOUGH is a shared-cost project (contract EVG1-CT-2002-00080) cofunded by the Research DG of the European Commission within the RTD activities of the Environment and Sustainable Development subprogramme (5th Framework Programme). TEKES is the Finnish Funding Agency for Technology and Innovation. The authors are grateful for Hans van der Marel (Technical University of Delft, the Netherlands) for providing the SD observations. Observation modeling of RO data at the European Centre for Medium-range Weather Forecasts is funded as part of the EUMETSAT GRAS SAF.

## References

- Andersson, E., J. Pailleux, J.-N. Thépaut, J. R. Eyre, A. P. McNally, G. A. Kelly, and P. Courtier (1994), Use of cloud-cleared radiances in three-/four-dimensional variational data assimilation, *Q. J. R. Meteorol. Soc.*, **120**, 627–653.
- Bevis, M., S. Businger, T. Herring, C. Rocken, R. Anthes, and R. Ware (1992), GPS meteorology: Remote sensing of atmospheric water vapor using the global positioning system, *J. Geophys. Res.*, **97**(D14), 15,787–15,801.
- Bevis, M., S. Businger, S. Chiswell, T. A. Herring, R. A. Anthes, C. Rocken, and R. H. Ware (1994), GPS meteorology: Mapping zenith wet delays onto precipitable water, *J. Appl. Meteorol.*, **33**, 379–386.
- Chevallier, F., P. Lopez, A. M. Tompkins, M. Janisková, and E. Moreau (2004), The capability of 4d-var systems to assimilate cloud-affected satellite infrared radiances, *Q. J. R. Meteorol. Soc.*, **130**, 917–932.
- de Haan, S., H. van der Marel, and S. Barlag (2002), Comparison of GPS slant delay measurements to a numerical model: Case study of a cold front passage, *Phys. Chem. Earth*, **27**, 317–322.
- Derber, J. C., and W.-S. Wu (1998), The use of TOVS cloud-cleared radiances in the NCEP SSI analysis system, *Mon. Weather Rev.*, **126**, 2287–2299.
- Doviak, J. D., and D. S. Zrnić (1993), *Doppler Radar and Weather Observations*, 562 pp., Elsevier, New York.
- Elgered, G., H.-P. Plag, H. van der Marel, S. Barlag, and J. Nash (Eds.) (2005), *COST Action 716: Exploitation of Ground-Based GPS for Operational Numerical Weather Prediction and Climate Applications. Final Report*, Rep. EUR 21639, European Union, 234 pp., COST Office, Brussels, Belgium.
- Eresmaa, R., and H. Järvinen (2006), An observation operator for ground-based GPS slant delays, *Tellus, Ser. A and Ser. B*, **58A**, 131–140.
- Eresmaa, R., H. Järvinen, S. Niemelä, and K. Salonen (2007), Asymmetry of ground-based GPS slant delay data, *Atmos. Chem. Phys.*, **7**, 3143–3151.
- Feltz, W. F., W. L. Smith, H. B. Howell, R. O. Knuteson, H. Woolf, and H. E. Revercomb (2003), Near-continuous profiling of temperature, moisture, and atmospheric stability using the atmospheric emitted radiance interferometer (AERI), *J. Appl. Meteorol.*, **42**, 584–597.
- Gustafsson, N., L. Berre, S. Hörnquist, X.-Y. Huang, M. Lindskog, B. Navascués, K. S. Mogensen, and S. Thorsteinsson (2001), Three-

- dimensional variational data assimilation for a limited area model. Part I: General formulation and the background error constraint, *Tellus, Ser. A and Ser. B*, 53A, 425–446.
- Ha, S.-Y., Y.-H. Kuo, Y.-R. Guo, and G.-H. Lim (2003), Variational assimilation of slant path wet delay measurements from a hypothetical ground-based GPS network. Part I: Comparison with precipitable water assimilation, *Mon. Weather Rev.*, 131, 2635–2655.
- Healy, S., and J.-N. Thépaut (2006), Assimilation experiments with CHAMP GPS radio occultation measurements, *Q. J. R. Meteorol. Soc.*, 132, 605–623.
- Healy, S. B., J. R. Eyre, M. Hamrud, and J.-N. Thépaut (2007), Assimilating GPS radio occultation measurements with two-dimensional bending angle observation operators, *Q. J. R. Meteorol. Soc.*, 133, 1213–1227.
- Hofmann-Wellenhof, B., H. Lichtenegger, and J. Collins (2001), *GPS: Theory and Practice*, 5th ed., 384 pp., Springer, New York.
- Hugentobler, U., S. Schaer, and P. Frides (2001), *Bernese GPS Software Version 4.2*, Astronomical Institute of Berne, Switzerland.
- Järvinen, H., R. Eresmaa, H. Vedel, K. Salonen, S. Niemelä, and J. de Vries (2007), A variational data assimilation system for ground-based GPS slant delays, *Q. J. R. Meteorol. Soc.*, 133, 969–980.
- Le Marshall, J. F., L. M. Leslie, and W. L. Smith (2002), Initialisation using high spatial, temporal and spectral resolution satellite observations, *Adv. Space Res.*, 30, 2441–2446.
- Lindskog, M., et al. (2001), Three-dimensional variational data assimilation for a limited area model. Part II: Observation handling and assimilation experiments, *Tellus, Ser. A and Ser. B*, 53A, 447–468.
- Liu, H., and M. Xue (2006), Retrieval of moisture from slant-path water vapor observations of a hypothetical GPS network using a three-dimensional variational scheme with anisotropic background error, *Mon. Weather Rev.*, 134, 933–949.
- Niell, A. (1996), Global mapping functions for the atmosphere delay at radio wavelengths, *J. Geophys. Res.*, 101(B2), 3227–3246.
- Poli, P., and J. Joiner (2004), Effects of horizontal gradients on GPS radio occultation observation operators. Part I: Ray tracing, 2004, *Q. J. R. Meteorol. Soc.*, 130, 2787–2805.
- Rodgers, C. D. (2000), *Inverse Methods for Atmospheric Sounding, Theory and Practice*, 238 pp., World Scientific, Singapore.
- Saastamoinen, J. (1972), Atmospheric correction for the troposphere and stratosphere in radio ranging of satellites, in *The Use of Artificial Satellites for Geodesy, Geophys. Monogr. Ser.*, vol. 15, edited by S. W. Henriksen et al., pp. 247–251, AGU, Washington, D. C.
- Schmetz, J., P. Pili, S. Tjemkes, D. Just, J. Kerkmann, S. Rota, and A. Ratier (2002), An introduction to Meteosat Second Generation (MSG), *Bull. Am. Meteorol. Soc.*, 83, 977–992.
- Undén, P., L. Rontu, H. Järvinen, et al. (2002), *HIRLAM-5 Scientific Documentation*, available from HIRLAM-5 Project, SMHI, S-60176, HIRLAM-5 Project, Norrköping, Sweden, 144 pp.

---

R. Eresmaa and K. Salonen, Research and Development, Meteorology, Finnish Meteorological Institute, Erik Palménin aukio 1, P.O. Box 503, Helsinki FIN-00101, Finland. (reima.eresmaa@fmi.fi)

S. Healy, European Centre for Medium-ranged Weather Forecasts, Research Department, Data Division, Shinfield Park, Reading RG2 9AX, UK.

H. Järvinen, Research and Development, Climate Change, Finnish Meteorological Institute, Erik Palménin aukio 1, P.O. Box 503, Helsinki FIN-00101, Finland.